metals

MDPI

Article

Identification of the Parameter Values of the Constitutive and Friction Models in Machining Using EGO Algorithm: Application to Ti6Al4V

Nithyaraaj Kugalur Palanisamy [1,*], Edouard Rivière Lorphèvre [1], Maxime Gobert [2], Guillaume Briffoteaux [2], Daniel Tuyttens [2], Pedro-José Arrazola [3] and François Ducobu [1]

[1] Machine Design and Production Engineering Lab, Research Institute for Science and Material Engineering, University of Mons, 7000 Mons, Belgium; edouard.rivierelorphevre@umons.ac.be (E.R.L.); francois.ducobu@umons.ac.be (F.D.)

[2] Mathematics and Operational Research Department (MARO), University of Mons, 7000 Mons, Belgium; maxime.gobert@umons.ac.be (M.G.); guillaume.briffoteaux@umons.ac.be (G.B.); daniel.tuyttens@umons.ac.be (D.T.)

[3] Mechanical and Manufacturing Department, Faculty of Engineering, Mondragon Unibertsitatea, Loramendi 4, 20500 Arrasate-Mondragón, Spain; pjarrazola@mondragon.edu

* Correspondence: nithyaraaj.kugalurpalanisamy@umons.ac.be; Tel.: +32-653-740-92

Abstract: The application of artificial intelligence and increasing high-speed computational performance is still not fully explored in the field of numerical modeling and simulation of machining processes. The efficiency of the numerical model to predict the observables depends on various inputs. The most important and challenging inputs are the material behavior of the work material and the friction conditions during the cutting operation. The parameters of the material model and the friction model have a decisive impact on the simulated results. To reduce the expensive experimentation cost that gives limited data for the parameters, an inverse methodology to identify the parameter values of those inputs is suggested to potentially have data of better quality. This paper introduces a novel approach for the inverse identification of model parameters by implementing the Efficient Global Optimization algorithm. In this work, a method relying on a complete automated Finite Element simulation-based optimization algorithm is implemented to inversely identify the value of the Johnson–Cook (JC) parameters and Coulomb's friction coefficient correlatively, where the objective function is defined as minimizing the error difference between experimental and numerical results. The Ti6Al4V Grade 5 alloy material is considered as a work material, and the identified parameters sets are validated by comparing the simulated results with experimental results. The developed automation process reduces the computation time and eliminating human errors. The identified model parameters value predicts the cutting force as 169 N/mm (2% deviation from experiments), feed force as 55 N/mm (7% deviation from experiments), and chip thickness as 0.150 mm (11% deviation from experiments). Overall, the identified model parameters set improves the prediction accuracy of the finite element model by 32% compared with the best-identified parameters set in the literature.

Keywords: orthogonal cutting; constitutive models; parameters set; finite element modeling; automation; artificial intelligence; Bayesian optimization; Ti6Al4V; machine learning; surrogate model

check for updates

Citation: Kugalur Palanisamy, N.; Rivière Lorphèvre, E.; Gobert, M.; Briffoteaux, G.; Tuyttens, D.; Arrazola, P.-J.; Ducobu, F. Identification of the Parameter Values of the Constitutive and Friction Models in Machining Using EGO Algorithm: Application to Ti6Al4V. *Metals* **2022**, *12*, 976. https://doi.org/10.3390/met12060976

Academic Editors: Denis Benasciutti and Giovanni Meneghetti

Received: 25 April 2022
Accepted: 2 June 2022
Published: 6 June 2022

Publisher's Note: MDPI stays neutral with regard to jurisdictional claims in published maps and institutional affiliations.

Copyright: © 2022 by the authors. Licensee MDPI, Basel, Switzerland. This article is an open access article distributed under the terms and conditions of the Creative Commons Attribution (CC BY) license (https://creativecommons.org/licenses/by/4.0/).

1. Introduction

The virtual simulation of the manufacturing process is an interesting topic for many researchers. The conventional machining process is necessary in the manufacturing industry to produce high-precision parts. The wide application of machined parts and the high complexity involved in the machining of materials to achieve the desired shapes and properties has motivated researchers for decades [1]. The analytical and experimental

investigations provide certain information to develop the process, but still, this information are inadequate. Experimental analysis is highly expensive and time-consuming, and it is difficult to measure variables such as stresses, strain, and temperature distribution [2]. The significant advancement in computation technologies enables us to develop a numerical model of the orthogonal cutting process [1].

Finite Element (FE) modeling is the most prominent numerical modeling technique for the simulation of the orthogonal metal cutting process [3] and the high-speed grinding of titanium alloy [4]. The FE simulation of the chip-formation process replaces the expensive experimental test and predicts the difficult-to-measure variables and results with higher accuracy than an analytical model [5]. The modeling of the complex machining process by the FE model is quite challenging as it involves various inputs. The efficiency of the cutting model is dependent on the numerical parameters such as the formulation type (Lagrangian, Eulerian, Arbitrary Lagrangian-Eulerian, or Coupled Eulerian–Lagrangian), the quality of the mesh [6], boundary conditions, constitutive models [7], and contact conditions [8]. Accurate material models and friction conditions between the tool-chip are essential to obtain accurate and reliable results from the simulation [9]. A reliable flow of stress data which relates the large plastic strains (1–6) at the very high strain rates (10^6 s^{-1}) and very high temperatures (800 K to 1400 K) observed during the machining process is necessary to frame the model. In this work, the Ti6Al4V alloy, an expensive alloy commonly used alloy for its excellent properties in the aerospace, biomedical, and marine fields, is considered for cutting process simulation.

In numerical modeling of the machining process, many different material models are employed, and they are classified as empirical/phenomenological, physical-based, and hybrid models [8]. The empirical models are highly recommended for their robustness, lower number of parameters, and the large availability of data when compared with physical-based and hybrid models [8]. Likewise, many friction models are available which are directly associated with the behavior of the material [10]. However, the credibility of the material model and the friction model depends on the pertinent parameters involved in defining the behavior of the material during machining process. These material model parameters are determined using a direct method or an inverse method [1]. The direct method is the dedicated experimental tests to obtain information. The experimental methods use curve fitting techniques to describe the experimental data from quasi-static and dynamic material tests such as the Split Hopkinson Pressure Bar (SHPB) test [11].

Nevertheless, these experiments can reach a maximum strain of 0.5 and a strain rate near 10^3 s^{-1}, which is well below the strain of 3 and the strain rate above 10^6 s^{-1} that are encountered during the cutting process, which makes the extrapolation of data necessary [12]. Although the pin-on ring, open and closed tribometers [13] friction test is available to determine the friction characteristics during the cutting process, the information is uncertain due to the phenomena taking place at the tool–chip contact area [14]. In [15], Sahoo et al. worked on tool coating and its relation with friction coefficient. They stated that, due to the lower friction coefficient of the coating material, the stress, strain, and temperature generation and tool wear rate in the case of TiAlN-coated tools are comparatively lower than uncoated WC tools. This adds further arguments for considering optimizing the friction coefficient with the constitutive model parameters in the identification framework.

The inverse methods are mainly used to overcome the drawback of extrapolation. In this context, Ozel and Altan developed the earliest approach to inversely identify the parameters from the cutting process [16]. In their study, the authors claim that the method can achieve less than 10% deviation from the measured and simulated cutting forces by using the flow stress data from the low-strain and strain rate tests as an initial starting point. In [17], Shrot and Baeker employed the Levenberg–Marquardt algorithm to re-identify some of the parameters of the Johnson–Cook model.

In [18], Klocke et al. proposed an inverse approach to determine the JC material and damage parameters for AISI 316L stainless steel. To determine the model parameters, the lower and upper values that underestimated and overestimated the experimental results

were guessed, and the material model parameters were interpolated to find the best fit with the experimental data. Later, they adopted the same approach to determine the material model parameters of AISI 1045 and Inconel 718.

In [19], Bosetti et al. compared Pure NMM (Nelder–Mead method), r-NMM, and Hybrid (Genetic Algorithm and NMM) approaches to determine the five JC parameters and Tresca friction parameter of AISI 304 stainless steel. Deviations up to 113% have been observed between the simulated and experimental observables. The authors state that the range of validity is limited, and the number of simulations and computation time depend on the initial guess for the parameters. Denkena et al. utilized Particle Swarm Optimization (PSO) algorithm in conjunction with Oxley's machining theory [20]. This approach suffers from the drawback of using the assumption of Oxley's machining theory.

In recent times, Bergs et al. [21] adapted a gradient-free approach called the Downhill Simplex Algorithm (DSA) for the inverse identification of the material model parameters. In this approach, they investigated the method with the inverse reidentification of a set of initial material model parameters taken from the literature. He observed a close match between the target and the simulated process observables. The authors applied this approach to experimental data from AISI 1045 and claim that the results are in agreement with the experimental results [22]. Hardt et al. [23] investigated this approach to evaluate the robustness of the algorithm to determine the parameter set and revealed the drawbacks associated with the algorithm, such as the algorithm being stuck in local minima.

In [24], the authors also used the PSO meta-heuristic to determine the parameters of the JC model for AISI 1045 steel. In this approach, the authors bound the upper limit and lower limit with an empirical value and investigated different swarm sizes of the PSO algorithm. The authors claim the approach can inversely re-identify the parameters of the constitutive model in a few iterations when compared with his earlier work [23]. In [25], Hardt et al. extended his work to include the automation of the post-processing of the results and increased the number of observables in the objective function. The authors concluded that different parameter sets identified by the algorithm result in the prediction of identical temperature, stress, and strain profiles, highlighting the non-uniqueness.

In the literature, mostly the parameters of the constitutive model are considered for the inverse identification process. The optimization algorithms implemented in the literature for the inverse identification procedure is computationally expensive (9 to 30 days minimum in parallel computation domain [24]). In addition, automatized optimization procedures need to be improved to transfer and interpret the data more efficiently.

In this present work, an identification procedure is proposed to inversely identify the value of the Johnson–Cook (JC) parameters and the Coulomb's friction coefficient correlatively, with the objective function being to minimize the error difference between experimental and numerical results. The inverse identification problem is tackled with the Finite Element simulation-based optimization concept. This work is a novel approach to overcome the drawbacks stated in the literature for the inverse identification of parameters. The first novelty of the work is the implementation of a complete automatized routine to perform the surrogate-guided optimization procedure to identify the model parameters values in the context of machining process simulation. The optimization process is based on the Bayesian Optimization (BO) algorithm named Efficient Global Optimization (EGO).

The EGO algorithm, first introduced by Jones et al. [26], uses a surrogate model to approximate the objective function (i.e., the difference between simulation and experiment) and determine the value of a candidate point to be exactly evaluated with the simulator (i.e., the FE model). It consequently alleviates the time cost associated with optimization since only valuable candidate points are simulated. EGO rests on Gaussian Process (GP) surrogate models for their ability to provide both a prediction and a measure of uncertainty around it. This characteristic allows one to define an Acquisition Function (AF) that assesses the value of a candidate point before evaluation (with the time-consuming simulator). Intuitively, the AF can be seen as an agent deciding if a region of the search space is worth sampling or not. It is then responsible for the Exploration/Exploitation trade-off in

the optimization process. In the context of time-consuming objective function with low budget and no place for parallel evaluations, the sequential EGO algorithm seems to be appropriate [27] for this work. In addition, the influence of algorithm parameters such as the influence of weight, the number of initial points to train the surrogate model, and different sets of bounds are investigated in this work, which contributes to additional novelty to the paper.

The Machine Learning algorithm combined with automation makes an efficient Artificial Intelligence (AI) platform to identify the parameter's value of the models. The proposed AI platform is significant in identifying the best parameter's values for the JC constitutive and Coulomb's friction model to predict the observables with less deviation from experiments when compared with the best parameter set stated in the literature by Ducobu et al. [28]. In addition, the optimization procedure reduces the total computation time to a maximum of 8 days without the need for a parallel computing domain.

The paper is organized as follows: In Section 2, Materials and Methods, the constitutive and friction models of the surrogate-guided optimization theoretical background and the EGO algorithm used within this work are outlined, followed by the experimental reference. The Arbitrary Lagrangian–Eulerian Finite Element model implemented for the simulation of orthogonal cutting is given in Section 3. In Section 4, the FE simulation-based optimization procedure is discussed in detail, followed by the framing of the optimization problem and the methodology to investigate the algorithm. The numerical results are also presented and briefed in Section 4. The identified parameters' values are analyzed and their applicability for other cutting conditions is critically discussed in Section 5. The conclusions are drawn based on the significance of the optimization procedure and the identified parameter sets in Section 6.

2. Materials and Methods

2.1. Constitutive Model

Orthogonal cutting modeling involves the complex thermo-mechanical coupled material behavior, which relates the flow stress to strain, the strain rate, and the temperature. Material models are the most critical input that have a major impact on the accuracy of any FE simulation. This model describes the high strain rate and high-temperature flow stress response of metals in machining. These models should consider deformation variables such as the plastic strain, plastic strain rate, and temperature under macroscopic scale. The general form is given in Equation (1):

$$\sigma = \sigma(\varepsilon, \dot{\varepsilon}, T), \tag{1}$$

Many constitutive models have been developed and proposed for orthogonal cutting processes based on real industrial machining applications in which empirical models are considered for their flexibility in adapting for various materials [29].

Johnson–Cook Constitutive Model

The JC constitutive model [30] is a widely employed material models which relates the strain, the strain rate, and temperature under machining conditions. The large availability of data and its mathematical simplicity, low computation time, and low memory requirements lead to the wide exploitation of this model in machining process simulations.

The JC flow stress equation is expressed by combining the plastic term representing the strain-hardening effect as a function of strain in the first bracket, the viscous term representing the strain rate in the second bracket, and the thermal softening term in the third bracket. Its flow stress equation is represented by Equation (2):

$$\sigma = (A + B\varepsilon^n)\left[1 + Cln\left(\frac{\dot{\varepsilon}}{\dot{\varepsilon_0}}\right)\right]\left[1 - \left(\frac{T - T_{room}}{T_{melt} - T_{room}}\right)^m\right] \tag{2}$$

The JC equation is governed by the five material parameters values (A, B, C, m, n), and their values depend on the material subjected to the orthogonal cutting process. The parameters' values are determined from the flow stress data observed from the experiments. The yield stress of the material at a reference temperature gives the value of parameter A, parameter B is the modulus of strain hardening, n is the strain-hardening exponent, C is the strain rate sensitivity, and m is the thermal softening exponent. T is the current temperature, T_{melt} and T_{room} are the melting and the room temperatures, respectively, while $\dot{\varepsilon_0} = 1$ is the reference strain rate.

The parameters' values are taken mostly from dynamic experimental material tests such as Split Hopkinson Pressure Bar (SHPB) [16,31]. These parameters' values are extrapolated, as experimental data are inadequate to represent the deformation behavior of the material. This significantly gives rise to the proposition of numerous parameter sets for the same material [16,32]. In [32,33], the authors concluded and justified that the parameters' values have a significant impact on the simulated results by conducting extensive research.

Identifying the values of the parameters is still a major concern for the successful simulation of the orthogonal cutting process of Ti6Al4V alloy. Other than the JC model, many other material models have been developed by modifying the JC model to represent the unique behavior of a Ti6Al4V alloy. Calamaz et al. [34] incorporated strain-softening terms into the JC model to predict the segmented chip in the orthogonal cutting simulation of a Ti6Al4V alloy. Sima and Özel [35] made some modifications to better control the thermal softening effect. However, this model involves more parameters, and these parameters are determined by fitting a curve between the measured and the predicted results from orthogonal cutting tests, without considering the material characterization. Nevertheless, due to the limited number of parameters and the wide availability and applicability of the JC model, it has been selected for this work. The novel method for inverse identification of parameters value to determine the JC model parameters presented in this paper is applicable to any material model.

2.2. Friction Model

In addition to the material model, the simulation results of the orthogonal cutting model significantly depend on the friction conditions [9]. Along with the material model and its parameters, the friction model coefficient between the tool and chip is another important problem that needs to be taken into consideration for successful simulation [1,8,36]. In [8], the authors conducted extensive research on the importance of friction conditions in modeling the cutting process. In these articles, many friction models are compared, and their applications to numerical simulation have been critically discussed. To name a few, Coulomb's friction, Velocity-dependent friction, Sticking-sliding friction models (Zorev's model) are some notable models employed in machining process modeling.

Coulombs Friction

In this work, Coulomb's (or Sliding) friction model is considered to define the friction conditions at the tool–chip interface. The classical Coulomb's friction model states that the frictional sliding force is proportional to the applied normal load. The coefficient of friction μ is termed as the ratio of the frictional sliding force to the applied normal force. The coefficient of friction is constant in all the contact lengths between the chip and tool. The Coulomb's friction law is given in Equation (3):

$$\tau = \mu\sigma \tag{3}$$

Even though it has been criticized by the researchers [29], Coulomb's model is still extensively employed for its simple mathematical expression and the good qualitative trends it provides. To determine the friction characteristics during the cutting process, experimental methods such as pin-on ring and open tribometer friction tests are available. However, the information is inadequate and uncertain due to complex phenomena taking

place at the tool–chip contact area [8,14]. Therefore, the friction parameters of the Coulomb's model are not reliable. In [9], the authors justify the importance of optimizing the friction coefficient value in correlation with the material model parameter value to have a better prediction on the observables through orthogonal cutting simulation.

2.3. Surrogate-Guided Optimization

JC model and Coulomb's friction parameters are optimized so that the numerical simulation is as close as possible to the physical experiment. Let us consider for now the inverse identification problem as an optimization problem taking the following form:

$$\min_{\boldsymbol{x}\in\Omega} f(\boldsymbol{x}), \tag{4}$$

where $\boldsymbol{x} \in \mathbb{R}^d$ is the decision vector including the model's parameters and $f : \mathbb{R}^d \to \mathbb{R}$; $\boldsymbol{x} \mapsto y = f(\boldsymbol{x})$ is the objective function representing the error function to be defined more precisely in the following. Considering that the objective function is time-consuming as it involves the numerical simulation, it is proposed to rely on a surrogate model in order to approximate the behavior of the objective function and alleviate the overall time-cost of the optimization process. Over the past years, BO has imposed itself as a reference approach for time-consuming optimization problems [37]. The strength of BO relies on its capability to select the next design point to be added to the data set. The candidate design point is selected not only according to the prediction provided by the surrogate model but also to its uncertainty. Indeed, BO uses a probabilistic model, mostly GP regression models, that provides a distribution of probability for each potential design point.

2.3.1. Gaussian Process Regression Surrogate Model

Following the description of Rassmussen and Williams in [38], let us assume that the simulator's output value y can be modeled by the following linear model:

$$y = \boldsymbol{\omega}^T \boldsymbol{x} + \varepsilon. \tag{5}$$

In GP, the weights $\boldsymbol{\omega}$ follow a Gaussian distribution, $\boldsymbol{\omega} \sim \mathcal{N}(0, \Sigma)$, which constitutes the prior belief. The ε noise is also assumed to be Gaussian $\mathcal{N}(0, \sigma^2)$. Given the data, the posterior distribution over the weights can be expressed using the Bayes rule as:

$$p(\boldsymbol{\omega}|\boldsymbol{X}, \boldsymbol{y}) = \frac{p(\boldsymbol{y}|\boldsymbol{X}, \boldsymbol{\omega})p(\boldsymbol{\omega})}{p(\boldsymbol{y}|\boldsymbol{X})} = \frac{p(\boldsymbol{y}|\boldsymbol{X}, \boldsymbol{\omega})p(\boldsymbol{\omega})}{\int_{\boldsymbol{\omega}} p(\boldsymbol{y}|\boldsymbol{X},\ \boldsymbol{\omega})p(\boldsymbol{\omega})d\boldsymbol{\omega}}. \tag{6}$$

The term $p(y|\boldsymbol{X})$ is often referred to as the evidence and can be expressed as the marginal likelihood by marginalizing over the weights $\boldsymbol{\omega}$.

Input data $\boldsymbol{X}$ can be projected into a feature space using a set of basis functions $\Phi(\boldsymbol{x}) = (\phi_1(\boldsymbol{x}), \ldots, \phi_k(\boldsymbol{x}))^T$, which leads to the following model: $y = \boldsymbol{\omega}^T\Phi(\boldsymbol{x}) + \varepsilon$. Denoting $\boldsymbol{\Phi} = \Phi(\boldsymbol{X})$, Equation (6) can be written replacing $\boldsymbol{X}$ by $\boldsymbol{\Phi}$. Knowing the distribution of the posterior $p(\boldsymbol{\omega}|\boldsymbol{\Phi}, y) \sim \mathcal{N}\left(\frac{1}{\sigma^2}A^{-1}\boldsymbol{\Phi}\boldsymbol{y}, A^{-1}\right)$ with $A = \sigma^{-2}\boldsymbol{\Phi}\boldsymbol{\Phi}^T + \Sigma^{-1}$, it is possible to make inference. The predictive distribution of a design point $\boldsymbol{x}^*$ can be written as:

$$\begin{aligned} p(y^*|\boldsymbol{\Phi}, \boldsymbol{y}, \boldsymbol{x}^*) &= \int_{\boldsymbol{\omega}} p(y^*|\boldsymbol{\omega})p(\boldsymbol{\omega}|\boldsymbol{\Phi}, \boldsymbol{y})d\boldsymbol{\omega} \\ &\sim \mathcal{N}\left(\frac{1}{\sigma^2}\Phi(\boldsymbol{x}^*)^T A^{-1}\boldsymbol{\Phi}\boldsymbol{y}, \Phi(\boldsymbol{x}^*)^T A^{-1}\Phi(\boldsymbol{x}^*)\right), \end{aligned} \tag{7}$$

and is also Gaussian. It can be shown that Equation (7) can be equivalently written as:

$$\begin{aligned} p(y^*|\boldsymbol{\Phi}, \boldsymbol{y}, \boldsymbol{x}^*) \sim \mathcal{N}\big(&\Phi(\boldsymbol{x}^*)^T\Sigma\boldsymbol{\Phi}(K + \sigma^2 I)^{-1}\boldsymbol{y}, \\ &K^{**} - K^{*\cdot}(K + \sigma^2 I)^{-1}K^{\cdot *}\big), \end{aligned} \tag{8}$$

where $K = \mathbf{\Phi}^T \Sigma \mathbf{\Phi}$ is known as the covariance matrix and $K^{(1)(2)} = \Phi(\boldsymbol{x}^{(1)})^T \Sigma \Phi(\boldsymbol{x}^{(2)}) = k\left(x^{(1)}, x^{(2)}\right)$. The k function is referred to as the covariance kernel and

$$K = \left(k(\boldsymbol{x}^{(i)}, \boldsymbol{x}^{(j)})\right)_{i,j \in \{1,\ldots,n\}}$$

as the covariance matrix. Hence, K^{**} denotes $k(\boldsymbol{x}^*, \boldsymbol{x}^*)$ and $K^{*\cdot}$ the row vector composed of $k(\boldsymbol{x}^*, \boldsymbol{x}^{(j)}) \forall j, j = 1, \ldots, n$. The kernel function is of particular importance and is chosen as an hyper-parameter among a family of kernel functions. The choice of the kernel is investigated in the experimental section.

2.3.2. Efficient Global Optimization Algorithm

In EGO, the surrogate model is used to propose a new candidate point by optimizating the AF, which is Expected Improvement (EI). The EI function is stated as follows in Equation (9):

$$EI(\boldsymbol{x}) = (y^* - y_{pred}(\boldsymbol{x}))\Phi\left(\frac{y^* - y_{pred}(\boldsymbol{x})}{\sigma(\boldsymbol{x})}\right) + \sigma(\boldsymbol{x})\phi\left(\frac{y^* - y_{pred}(\boldsymbol{x})}{\sigma(\boldsymbol{x})}\right), \tag{9}$$

where y^*, $y_{pred}(x)$, $\sigma(x)$ stand for the best current objective value, the prediction of $\boldsymbol{x}$ from the surrogate model, and its standard deviation, respectively. Φ is the cumulative density function of $\mathcal{N}(0,1)$, and ϕ is the corresponding probability density function. The important thing to be noticed is that EI will be high if σ is high (high uncertainty, hence high potential of improvement for the surrogate model) and also if the prediction is low compared to y^* (in case of minimization). EI is consequently responsible for the trade-off between exploration and exploitation in the optimization process.

Algorithm 1 shows the essential steps of the EGO algorithm. Given the hyper-parameters relative to the surrogate model and the AF, the optimization process is initialized with a first set of points evaluated with the simulator, named the Design of Experiment (DoE) at line 1. A GP model is fitted with this data set at line 3 in order to select the next point to be evaluated thanks to the optimization of the AF displayed at line 4. Once this candidate is chosen, it is evaluated with the time-consuming simulator and integrated into the data set as shown at line 6. Lines 3 to 6 are referred to as a cycle and operate, respectively, until the allocated budget runs out.

Algorithm 1 Efficient Global Optimization algorithm.

1: Initial DoE: $\mathcal{D} = \{\boldsymbol{X}, \boldsymbol{y}\}$
2: **while** Budget available **do**
3: $\quad \mathcal{M} = \mathcal{GP}(\Omega)$
4: $\quad \boldsymbol{x}_{new} = argmax_{\mathcal{D}}(EI(\boldsymbol{x}))$
5: $\quad y_{new} = f(\boldsymbol{x}_{new})$
6: $\quad (\boldsymbol{X}, \boldsymbol{y}) = (\boldsymbol{X}, \boldsymbol{y}) \cup (\boldsymbol{x}_{new}, y_{new})$
7: **end while**

2.4. Experimental Reference

The experimental work from Ducobu et al. [39] is considered for this work. The orthogonal cutting experiments were performed with Ti6Al4V with the same cutting condition as the model for uncut chip thickness of 0.1 mm is considered as a reference for this study. The experimental setup proposed by Ducobu et al. [39] aims to remove a layer of material that resembles the orthogonal configuration. Each cutting test was performed for 0.02 s, the time required to travel the 10 mm length. The orthogonal cutting configuration is given in the Figure 1.

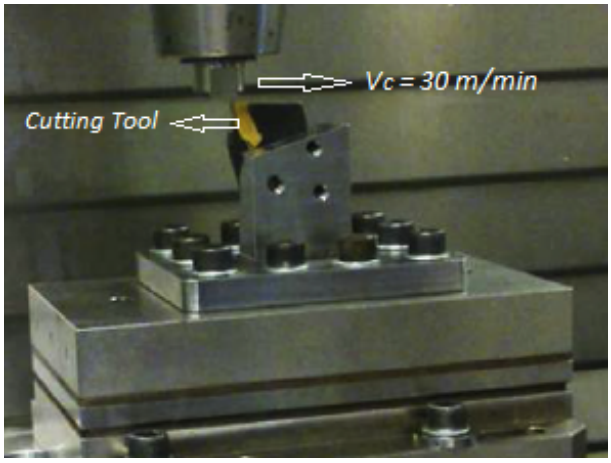

Figure 1. Cutting configuration on the milling machine.

The cutting conditions of the experimental tests conducted by Ducobu et al. [39] are given in Table 1.

Table 1. Cutting conditions of the experiments.

Cutting speed (m/min)	30	
Uncut chip thickness (mm)	0.1	6 repetitions
Width of cut (mm)	1	
Length of cut (mm)	10	
Rack angle (°)	15	
Clearance angle (°)	2	
Cutting edge radius (mm)	0.02	

To guarantee the repeatability of the tests, 6 repetitions were performed. The forces were measured with a Kistler 9257B dynamometer (Kistler Ibérica S.L, Barcelona, Spain) and a useful part of the signal during cutting operation was considered to compute the RMS value of forces. The chips from the orthogonal cutting were observed with an optical microscope to measure the cut chip thickness.

A continuous chip was observed from the orthogonal cutting experiment for an uncut chip thickness of 0.1 mm. The chip observed from the experiment is shown in Figure 2. The experimental outputs are given in Table 2.

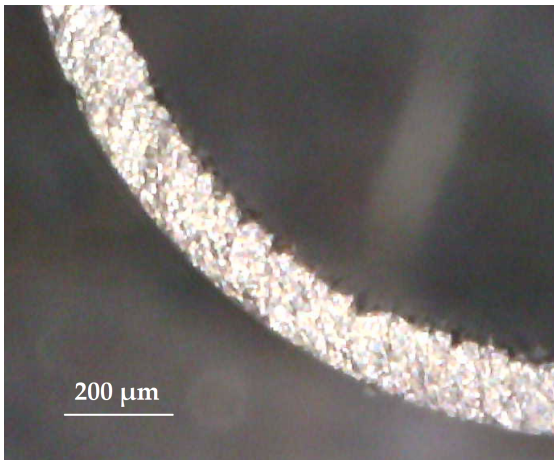

Figure 2. Experimental reference chip morphology for uncut chip thickness of 0.1 mm.

Table 2. Experimental results summary (6 repetitions for h = 0.1 mm).

h (mm)	F_c (N/mm)	F_f (N/mm)	h' (mm)
0.1	173 ± 2	51 ± 1	0.135 ± 0.006

3. Finite Element Orthogonal Cutting Model

In FE modeling, the Eulerian and the Lagrangian formulations [1,5] are usually considered. In the Eulerian approach, the computational mesh is fixed, and the material moves with respect to the grid, which allows handling large distortions. Prior information on the chip geometry is required to model the machining simulations with the Eulerian formulation [1], and it is adopted only for steady-state chip formation. In Lagrangian formulation, the nodes of the mesh are attached to the material and follow the material's deformation. It may induce large distortions in the domain, and frequent remeshing operations may be necessary to adapt large deformations. In addition, without remeshing, the Lagrangian formulation needs chip separation criteria [5].

To overcome the drawbacks of the purely Eulerian and purely Lagrangian formulations, two other formulations which combine the merits of Lagrangian and Eulerian have been developed. They are the Arbitrary Lagrangian–Eulerian (ALE) and the Coupled Eulerian–Lagrangian (CEL) formulations. In the ALE formulation, the material flows through the mesh like in the Eulerian formulation. Because of this freedom in movement of the mesh, the ALE description can accommodate high distortions with more resolution [40]. In the CEL formulation, a Lagrangian part is modeled within a Eulerian domain, and the efficiency of the model depends on the Eulerian mesh definition; no mesh distortion occurs [6].

In this work, an explicit ALE finite element formulation was adopted to simulate the orthogonal cutting process of Ti6Al4V. This ALE formulation combines the advantage of Lagrangian and Eulerian formulations, which allows one to take into account the large deformations during the material flow around the cutting edge of the tool without using a chip separation criterion. A two-dimensional (2D) plane strain model with orthogonal cutting assumption was considered for this work. The finite element software Abaqus was used to model the thermo-mechanical chip formation process.

In this FE model, the tool is fixed, and the workpiece moves at the prescribed cutting speed. The tool and the workpiece are meshed with quadrilateral elements with reduced integration for a coupled temperature–displacement calculation (CPE4RT). The length of the workpiece is 3 h, where h is the uncut chip thickness. To achieve a better trade-off between the element size and computation time, the area near the cutting zone (near the tool-tip) was modeled with a finer mesh of size 5 µm. In this approach, the initial geometry of the chip must be predefined with respect to the uncut chip thickness (h). The workpiece inflow and outflow surfaces, as well as the chip top surface, were modeled as Eulerian surfaces, and adaptive constraints were applied. For the tool, tungsten carbide was considered, and the linear elastic law was imposed [41]. The chemical composition of Ti6Al4V is given in Table 3.

Table 3. Chemical Composition of Ti6Al4 V [42].

Element	Al	C	Fe	H	0	N	V	Ti
Composition (mass %)	6	0.1	0.4	0.015	0.05	0.2	3.5–4.5	Balance

The material properties of Ti6Al4V considered for this work are given in Table 4.

Table 4. Material properties considered for this study [43,44].

Material Properties	Ti6Al4V	Tungsten Carbide
Young's modulus (GPa)	113.8	800
Density (kg/m^3)	4430	15,000
Poisson's ratio	0.342	0.2
Expansion (K^{-1})	8.6×10^{-6}	4.7×10^{-6}
Conductivity (W/mK)	7.3	46
Specific heat (J/KgK)	580	203
Inelastic heat fraction	0.9	
Hardness [Rockwell C]	41	

The tool geometry and the cutting conditions are given in Table 5.

Table 5. Cutting conditions.

Cutting and Tool Parameters	Values
Cutting speed (m/min)	30
Uncut chip thickness (mm)	0.1
Rack angle (°)	15
Clearance angle (°)	2
Cutting edge radius (mm)	0.02

The initial geometry and the boundary conditions are illustrated in Figure 3. The thermal properties are adopted from the literature [44,45]. The initial temperature for tool and work piece is set to 298 K. The mass scaling was considered to artificially increase the critical time increment in the simulations. A mass scaling factor of 1000 was considered, as it shows a significant decrease in the computational time without affecting the results [28]. This approach is crucial to reach the steady state (it is enough in these cutting conditions) for force calculations with less computation time (42 min with 6 cores Intel® Core™ i7-10700 CPU @2.90 GHz with the memory of 16 GB). The specifications of the PC machine used for the FE simulations are given in Table 6.

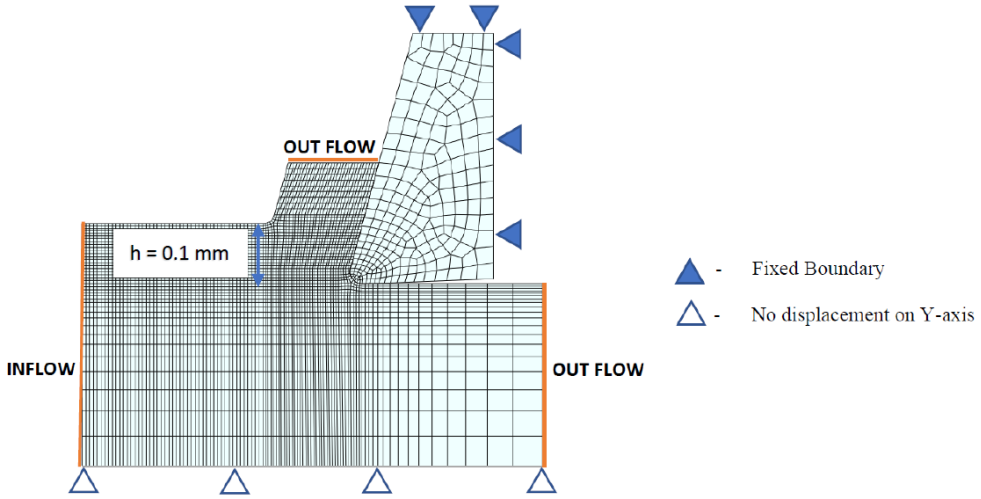

Figure 3. Finite element model with initial geometry, initial mesh structure, and boundary conditions.

Table 6. PC machine specification.

Memory	16 GB
CPU	Intel® Core™ i7-10700 CPU @2.90 GHz
No. of cores	6 cores

The reaction forces and the chip characteristics from the FE simulation were processed to calculate the cutting force, feed force, and the chip thickness

3.1. Post-Processing Automation

A post-processing automation script has been created. It investigates the output file (.ODB in Abaqus) stored in a specific folder after processing the input file and the completion of the computation. This post-processing is the crucial part, where the information from the specific nodes is examined and mathematical works (such as Root Mean Square calculations of forces and euclidean distance between the chip sides) are carried out to determine the desired results. In the orthogonal cutting simulation, the cutting force, feed force, and chip thickness are usually analyzed and are compared with the experimental results.

The cutting force and feed force were evaluated by considering the average value in the steady-state. The information on the coordinate points of the chip was required to calculate the chip thickness. The chip produced by the simulation was continuous (it has the shape of a curve). The direct measurement of the chip thickness was unlikely due to the shape of the chip. Both sides of the chip were modeled with Bézier curves, and the chip thickness was measured as an average of distance between those curves evaluated on several points. In addition, kinetic energy vs. internal energy information was acquired to check the stability of the ALE model with mass scaling. The post-processing script helps to analyze the result faster and more accurately.

3.2. Numerical Simulation and Results

The numerical results for the uncut chip thickness of h = 0.1 mm are investigated with the JC parameters identified by Seo et al. [46] and Coulomb's friction coefficient of 0.2 from Arrazola et al. [1]. The parameters set adopted for the numerical simulation is given in Table 7.

Table 7. Parameters set adopted [1,46].

Parameters	Values
A (MPa)	997.9
B (MPa)	653.1
C	0.0198
m	0.7
n	0.45
μ	0.2
T_{room} (K)	298
T_{melt} (K)	1878

The morphology of the numerically simulated chips was continuous, as in the experimental reference. The temperature distribution of numerical chips is given in Figure 4a. As expected, the temperature is maximum in the secondary deformation zone for all the numerical chips. This confirms the fact that the heat transfer in the machining process takes place primarily in the shear zones, where the plastic work is converted into heat and at the chip–tool interface, where frictional heat is generated.

The temperature fraction between the work piece, tool, and chip was also obeserved. For all the numerical chips, high plastic strain around 3.5 is observed at the chip side in contact with the tool rake face. The Equivalent Plastic strain (PEEQ) contour is given in Figure 4b.

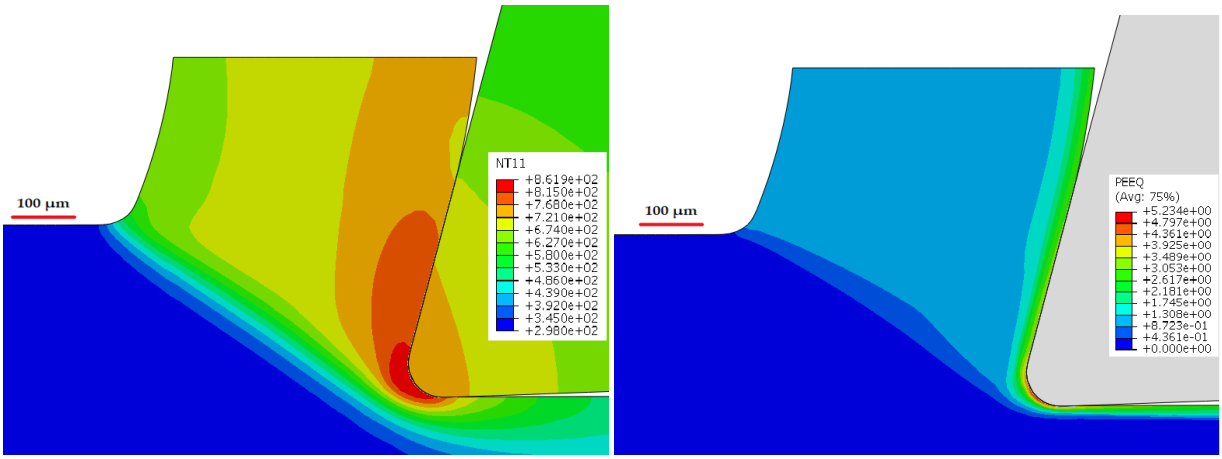

(**a**) Temperature Contour with Temperature Scale (**b**) PEEQ contour with PEEQ Scale

Figure 4. (**a**) Temperature contour (in K) with temperature scale; (**b**) Equivalent Plastic strain (PEEQ) contour with PEEQ Scale for h = 0.1 mm at 4 ms of cutting time.

The Root Mean Square (RMS) values of the cutting force and feed force were investigated through automation script and are given in Table 8.

Table 8. RMS cutting force (F_c), feed force (F_f), chip thickness (h'), and Δx differences with the experimental values.

Uncut Chip Thickness h (mm)	Models	F_c (N/mm)	ΔF_c (%)	F_f (N/mm)	ΔF_f (%)	h' (mm)	$\Delta h'$ (%)
0.1	Experiment	173 ± 2	-	51 ± 1	-	0.135 ± 0.006	-
	Seo et al. [46]	177	2	41	22	0.177	27

The forces were evaluated at their steady-state to calculate the RMS value. The plot between forces vs. time, representing both the total and steady-state evolution, is shown in Figure 5a. The evaluation of chip thickness is given in Figure 5b. The plot between kinetic energy vs. internal energy to show the ratio of kinetic energy to the internal energy is less than 5%, which determines the stability of the ALE model, is given the Figure 5c.

The results from the numerical analysis show that the ALE model is well defined. The RMS value of the cutting force from JC with the parameters identified by Seo et al. [46] and Coulomb's friction coefficient of 0.2 are very close to the experimental ones, with a small deviation of 2%, whereas the feed force and the chip thickness are in the deviation of 22 to 27%. The above analysis depicts the fact that the ALE model is suitable to obtain qualitative results. This shows that the ALE model is relevant to be incorporated in an FE simulation-based optimization algorithm for the inverse identification of parameters.

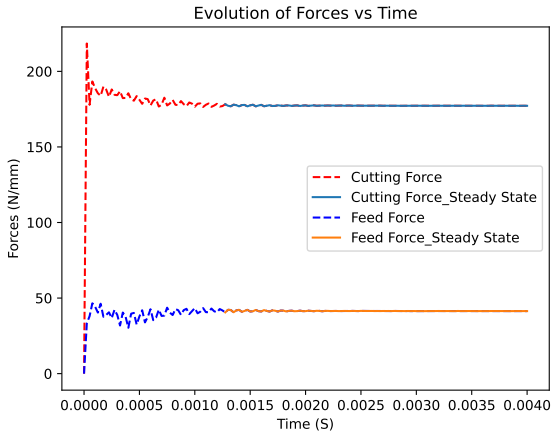

(**a**)

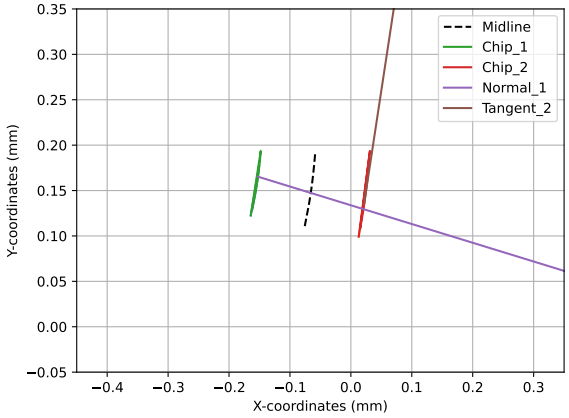

(**b**)

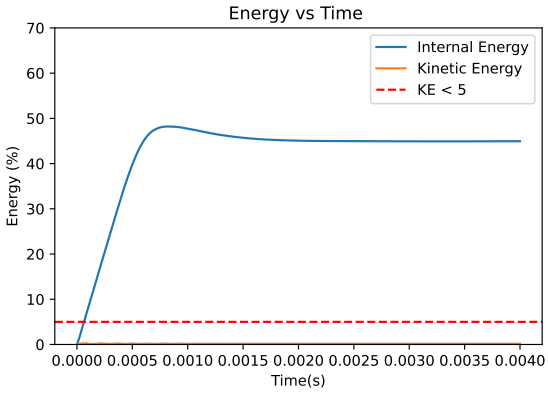

(**c**)

Figure 5. Result analysis for the Seo model ($h = 0.1$ mm): (**a**) Force Evolution vs. Time plot; (**b**) Chip Thickness Evaluation plot; (**c**) ALE Model Stability Analysis plot.

4. Methodology: Machining Simulation Based Optimization

In this work, the EGO algorithm was employed to inversely determine the parameters' value of the JC constitutive model and of the Coulomb's friction coefficient. The FE model of the orthogonal cutting process of the Ti6Al4V alloy is denoted as the simulator, and EGO was used to minimize the deviation between simulated results and the experimental results.

The algorithm was completely automated to eliminate human intervention, and following the scheme presented in Algorithm 1, the following steps were carried out:

1. Generation of the initial set of design points according to the Latin Hypercube Sampling (LHS) space filling methodology;
2. Processing of the initial design points to find the observables (F_f, F_c, h') via numerical simulator;
3. Evaluation of the objective function according to the observables;
4. Building of the GP surrogate model to approximate the objective function;
5. Optimization of the AF yielding new design point;
6. Evaluation of the new design point (numerical simulation and objective function);
7. Integration of the new design point in the data set;
8. Steps 4 to 7 are repeated until the budget runs out.

4.1. Problem Definition

The JC model parameters (B, C, n, m) and the Coulomb friction parameters (μ) are expressed as design variables, input variables, or decision vectors of the optimization problem. Parameter A is the yield stress in JC model. To realize the mechanical properties of the Ti6Al4V, the yield stress parameter value A of Ti6Al4V in the JC model was set to 997.9 MPa [43,46]. It is therefore not included in the variable.

Hence, the decision vector of the optimization problem is given in Equation (10):

$$\boldsymbol{x} = \begin{pmatrix} B & C & m & n & \mu \end{pmatrix} \in \mathbb{R}^5 \tag{10}$$

The objective function is defined based on minimizing the deviation in the FE numerical simulation outcomes: the cutting force ${F_c}^{(sim)}$, feed force ${F_f}^{(sim)}$, and chip thickness ${h'}^{(sim)}$ with experimental (physical) outcomes and cutting force ${F_c}^{(exp)}$, feed force ${F_f}^{(exp)}$, chip thickness ${h'}^{(exp)}$ for the uncut chip thickness $h = 0.1$ mm. The weighted sum method was considered in this study, which allowed the multi-objective problem to act as a single objective mathematical problem. This real-value objective function is given in Equation (11):

$$F(\boldsymbol{x}) = w_{F_c} \frac{|{F_c}^{(sim)} - {F_c}^{(exp)}|}{\max|{F_c}^{(sim)} - {F_c}^{(exp)}|} + w_{F_f} \frac{|{F_f}^{(sim)} - {F_f}^{(exp)}|}{\max|{F_f}^{(sim)} - {F_f}^{(exp)}|} + w_{h'} \frac{|{h'}^{(sim)} - {h'}^{(exp)}|}{\max|{h'}^{(sim)} - {h'}^{(exp)}|} \tag{11}$$

where w_i represents the weight coefficient of individual observables with $(\sum w_i = 1)$. The weight of an observable is chosen according to its application. In this work, two different sets of weight coefficients $\boldsymbol{w} = (w_{F_c}, w_{F_f}, w_{h'})$ are investigated to determine their influence in identifying the parameter values. The first set of weights, $\boldsymbol{w^{(1)}} = (1/3, 1/3, 1/3)$, is a uniform distribution on the three observable contributions (F_c, F_f, h'). The second set of weights, $\boldsymbol{w}^{(2)} = (0.40, 0.35, 0.20)$ gives more weight to the cutting force F_c than feed force F_f and less weight to chip thickness h' to take into account the hierarchy of the observables for cutting process optimization in an industrial context.

The parameters to be identified were limited within meaningful physical boundaries. Two sets of bounds have been considered for the JC parameters (B, C, m, n) in this study. The first set of bounds (B_1) are the upper and lower value of the bounds are chosen from the work of Ducobu et al. [32], where the authors extensively investigated the available sets of parameters in the literature for Ti6Al4V alloy. The second set of bounds (B_2) were the upper and lower bounds are chosen empirically with in the physical limit of the TI6Al4V alloy to study the influence of bounds. A single bound is chosen for a friction coefficient is chosen within physical meaning $(\mu \in [0, 1])$. The two sets of bounds are given in Tables 9 and 10.

Table 9. First Set of Bounds (B_1).

Parameters	Lower Limit	Upper Limit
B (MPa)	331.2	1092
C	0.000022	0.05
m	0.6437	1.51
n	0.122	1.01
μ	0	1

Table 10. Second Set of Bounds (B_2).

Parameters	Lower Limit	Upper Limit
B (MPa)	300	1100
C	0.00001	0.06
m	0.5	1.55
n	0.1	1.1
μ	0	1

The numerical simulator (Abaqus) used to compute the observables for each design point is computationally expensive. Indeed, the computation time to obtain the results for the uncut chip thickness h = 0.1 mm for one complete simulation is about 42 min. Increasing the number of initial design points will proportionally increase the total computation time. To determine the number of initial points to obtain qualitative results from the optimization algorithm, an investigation has also been carried out to analyze the influence of the number of initial design points.

4.2. Optimization Methodology

Following common recommendations of BO [26], an initial data set containing 60 ($12 \times d$, with the problem dimension $d = 5$) design points was generated according to the LHS approach [47] in order to ensure a good space filling. Based on this initial data set, an analysis is conducted to explore various combinations of hyper-parameters for the GP model. The procedure involves several kernels and mean functions for the model, as well as various learning rates for the optimization of the model. A grid search is performed among the mentioned parameters within the objective of identifying the best model's hyper-parameters according the Leave-One-Out Cross-Validation score [48]. All the experiments are performed using the GPyTorch framework in Python [49] and revealed that the constant mean and spectral mixture kernel achieves good results with a learning rate of 0.1.

The AI-based concept involving the optimization algorithm (ML algorithm) and automation makes the decision on the best parameter sets for the JC and Coulomb's friction model efficiently. AI reduces the time taken to perform optimization runs and human errors. Different optimization runs for inverse identification of the JC constitutive model and Coulomb's friction model are carried out utilizing the advantage of AI. Table 11 presents the four optimization models.

Table 11. Optimization Methodology—Algorithm Models.

Optimization Model	No. of Initial Points	Weight Coefficients	Bound Set
M_1	60	$\boldsymbol{w^{(1)}} = (1/3, 1/3, 1/3)$	B_1
M_2	60	$\boldsymbol{w^{(2)}} = (0.40, 0.35, 0.20)$	B_1
M_3	10	$\boldsymbol{w^{(1)}} = (1/3, 1/3, 1/3)$	B_1
M_4	10	$\boldsymbol{w^{(1)}} = (1/3, 1/3, 1/3)$	B_2

All the optimization models were run on the same machine (therefore, with the same computational power). In a PC, parallel computing is already used inside the simulator (Abaqus) in order to reduce the computation time of a single simulation. Then, sequential EGO is preferred to parallel versions [27,50].

The parameter sets identified by the model M_1 and the relevant information are given in Table 12. The characteristics of models M_2, M_3, and M_4 are given in Table 11, and relevant information on their objective values and computation times is given in Table 12.

Table 12. Identified parameter sets by the Efficient Global Optimization algorithm Models.

Optimization Models	B (MPa)	n	m	C	μ	Objective Value	Computation Time
M_1	331.2	0.594	0.6434	0.050000	0.19	0.019	8 days 2 h
M_2	331.2	0.620	0.6437	0.050000	0.24	0.021	8 days 4 h
M_3	356.0	0.323	0.6834	0.045286	0.12	0.017	7 days 8 h
M_4	434.4	0.187	1.4761	0.008613	0.07	0.022	7 days 10 h

4.3. Numerical Results

The optimized values from the EGO algorithm for the JC model and the Coulomb's friction coefficient parameters are employed to build the FE model. The results from these

FE simulations are compared with the experimental results for validation of the identified parameters. The RMS values of the forces and the chip thickness for uncut chip thickness $h = 0.1$ mm considering the influence of the algorithm parameters are given in Table 13.

Table 13. RMS cutting force (F_c), feed force (F_f), chip thickness (h'), and Δx differences with the experimental results for h = 0.1 mm.

Uncut Chip Thickness h (mm)	Models	F_c (N/mm)	ΔF_c (%)	F_f (N/mm)	ΔF_f (%)	h' (mm)	$\Delta h'$ (%)	Δ_{Total} (%)
0.1	Experiment	173 ± 2	-	51 ± 1	-	0.135 ± 0.006	-	-
	Seo et al. [46]	177	2	41	22	0.177	27	51
	M_1	163	6	53	4	0.147	9	19
	M_2	169	2	55	7	0.150	11	20
	M_3	157	10	55	8	0.134	1	19
	M_4	158	9	47	8	0.153	12	29

The influence of the algorithm parameters plays a significant role in identifying parameters. Nevertheless, the parameters identified by EGO with any algorithm parameters are able to predict the observables considered in this study with an overall deviation in the range of 19% to 29%, a significant improvement compared to the initial deviation of 51%. The deviation can further be reduced by increasing the number of iterations, which correspondingly increases the computation time.

With 300 iterations, models M_1 and M_2 perform better in predicting the cutting force and the feed force. The model M_2 predicts the cutting force within the deviation of 2%, as more weights are put on the cutting force than on the feed force and the chip thickness, whereas, in model M_1, the weights are equally distributed, which reflects the prediction of observables with a deviation of 6% and 4% for the forces and 9% for the chip thickness. M_3 with less initial design samples and with equally distributed weights predicts the observables with a total deviation of 19% but shows a high deviation for the cutting force (10%) and less deviation for the chip thickness (1%). As expected, model M_4 shows more deviation (29%) because of the increasing upper and lower bound values.

5. Discussion

The four optimization models (M_1, M_2, M_3, M_4) considered in this work perform well in determining the model parameters value with a maximum computation time of 8.5 days. Indeed, the total deviation of the simulated results from the experimental results lies in the range of 19% to 29%. The identified parameter sets from the optimization for the JC model along with the friction coefficient can predict the forces and the chip thickness 62% more efficiently than the best parameter sets determined by Ducobu et al. [32] (Their method was a critical investigation of the available parameter sets in the literature for the machining of Ti6Al4V alloys, and friction was not included).

In the machining process, knowledge about the forces is of utmost importance in optimizing the cutting process. Taking that into account, more interest is put on the forces' prediction with the identified parameter sets. The difference (Δ_x) of simulated results with the experimental results with respect to the forces is given in Table 14.

Table 14. RMS cutting force (F_c), feed force (F_f), and Δx differences with the experimental forces.

Uncut Chip Thickness h (mm)	Models	F_c (N/mm)	ΔF_c (%)	F_f (N/mm)	ΔF_f (%)	Δ_{Force} (%)
0.1	Experiment	173 ± 2	-	51 ± 1	-	-
	Seo et al. [46]	177	2	41	22	24
	M_1	163	6	53	4	10
	M_2	169	2	55	7	9
	M_3	157	10	55	8	18
	M_4	158	9	47	6	15

The parameters set found by the optimization models M_1 and M_2 predict the cutting force and feed force with less deviation from the experimental results when compared with models M_3 and M_4. Indeed, the cutting force predicted by the parameter sets identified by M_3 and M_4 is in the range of 9% to 10%, which is slightly more when compared with the reference parameter sets considered in this study [1,46]. However, the feed force predicted by the identified parameter sets by the optimization models M_3 and M_4 significantly reduces the deviation in the numerical results from the experimental results. The parameter set from M_2 predicts the cutting force near the experimental result, as the optimization model is defined with a greater weight coefficient on the cutting force than the feed force, which is reflected in the parameter identification process of the algorithm. Even though the parameter set from M_1 predicts the total forces with a deviation of around 10%, the cutting force deviation could be improved. This is due to the definition in the equal weight coefficients of the observables. The model M_3 predicts the forces with a deviation of 18% from the experimental results. Indeed, the identified parameter sets can predict the same chip thickness as the experimental reference but fail to predict the forces with less deviation from the experiments. The model M_4 predicts the forces with a deviation of 15%; this can be explained by the increase in the range of the B_2.

The JC parameter sets and the Coulomb's friction coefficient identified by the optimization models M_1 and M_2 are selected for further analysis, as they provide a good trade-off between the predicted forces and the chip thickness. Two other values of uncut chip thickness, h = 0.04 mm and h = 0.06 mm, are introduced to further analyze and validate the identified parameters from the optimization. The results from these FE simulations are compared with the experimental results. The RMS values of the forces and the chip thickness for uncut chip thicknesses of h = 0.04 mm and 0.06 mm are given in Table 15.

The identified parameter sets for the JC and Coulomb's friction coefficients by the M_1 and M_2 optimization models can accurately predict the cutting force (deviation within 4%) for uncut chip thicknesses of h = 0.04 mm and 0.06 mm. Meanwhile, the feed force is overestimated (16% to 33%). The chip thickness prediction shows some improvement when compared with the reference model, even though they are overestimated (14% to 19%) when compared with the experimental measurements.

The inversely identified parameters values of the JC model and Coulomb's friction coefficient value qualitatively predict the observables for the cutting condition considered for optimization. The accuracy is lower for the other cutting conditions but still quite good, particularly for the cutting force. However, this analysis on cutting conditions is different than the one conducted for the optimization, showing the limits of an optimization performed for a single cutting condition. Nevertheless, the prediction of the cutting forces with the identified parameter sets are in close agreement (<10%) with the industrial trends, where the cutting force prediction has fundamental importance for the optimization of cutting conditions, tool design, and also for tool wear/life prediction [1]. Indeed, the identified parameter sets can predict the cutting forces within a deviation of 6% for all the cutting conditions considered in this study, while Arrazola et al. [1] state that the experimental measurement trials and the variations in the material properties of the same material can cause variations of around 10% in forces.

Table 15. RMS cutting force (F_c), feed force (F_f), chip thickness (h'), and Δx differences with the experimental results for $h = 0.04$ mm and $h = 0.06$ mm.

Uncut Chip Thickness h (mm)	Models	F_c (N/mm)	ΔF_c (%)	F_f (N/mm)	ΔF_f (%)	h' (mm)	$\Delta h'$ (%)	Δ_{Total} (%)
0.06	Experiment	112 ± 2	-	45 ± 1	-	0.080 ± 0.004	-	-
	Seo et al. [46]	120	7	41	9	0.112	33	49
	M_1	112	-	56	22	0.093	15	37
	M_2	116	4	53	16	0.097	19	39
0.04	Experiment	86 ± 2	-	41 ± 1	-	0.059 ± 0.005	-	-
	Seo et al. [46]	92	7	35	16	0.083	34	57
	M_1	86	-	57	33	0.068	14	47
	M_2	88	2	52	24	0.071	18	44

6. Conclusions

In this research work, a novel approach introducing an automated FE-based Bayesian optimization algorithm for inverse identification of the parameters value of the JC model and Coulomb's friction model for orthogonal cutting FE modeling of Ti6Al4V alloy has been explored. The optimization procedure searches for the best parameter values for the JC model and Coulomb's friction model by minimizing the error between the numerical prediction and experimental data related to the cutting force, feed force, and chip thickness. To conclude, the applicability of the EGO algorithm for the inverse identification of parameters' values in the context of the orthogonal cutting of a Ti6Al4V alloy was successfully realized. The best parameter sets were identified by the optimization models M_1 and M_2. The identified parameter sets are incorporated in the FE modeling of the orthogonal cutting process and are validated with the experimental results. The following outcomes are drawn from the above study:

- The parameter sets identified by the EGO algorithm provide highly qualitative results for the cutting condition considered for optimization.
- The identified parameter sets from the optimization models M_1 and M_2 predicted cutting forces that are in close agreement with the experimental measurements, with deviations less than 10% for all the cutting conditions considered in this study.
- The parameter sets from the models M_1 and M_2, along with the ALE model developed in this work, predict the forces and chip thickness 31% more effectively for the considered cutting condition than the best parameter sets identified and stated in the literature.
- The feed force and chip thickness prediction had deviations of around 10% for an uncut chip thickness of h = 0.1 mm. However, for the uncut thicknesses of h = 0.06 mm and 0.04 mm, the feed force and the chip thickness are overestimated. Anyhow, the identified parameters predict the forces and chip thicknesses 13–10% more effectively than the best parameter sets identified and stated in the literature.
- Overall, the proposed algorithm is computationally efficient and reasonably accurate in predicting the observables. The algorithm procedure requires 8 days to complete the whole optimization process in a computing machine without the need for a parallel computing domain. These significant factors highlight its capability for implementation at the industry level.

Based on the analysis, either of the parameter sets from the optimization models M_1 or M_2 can be selected according to the user's interest in the observables. In the future, further investigation should be carried out to identify the model parameters via optimization by considering multiple cutting conditions. In addition, parallel computing can be used to reduce the optimization time or increase the budget in order to obtain better results within the same time.

Author Contributions: Conceptualization, N.K.P., F.D., E.R.L. and D.T.; methodology, N.K.P., M.G., G.B., F.D. and E.R.L.; software, N.K.P., M.G. and G.B.; validation, N.K.P. and M.G.; formal analysis, N.K.P.; investigation, N.K.P., M.G. and G.B.; resources, N.K.P., M.G., G.B., F.D., E.R.L. and D.T.; data curation, N.K.P., F.D. and E.R.L.; writing—original draft preparation, N.K.P. and M.G.; writing—review and editing, N.K.P., M.G., F.D., E.R.L., P.-J.A. and D.T. ; visualization, N.K.P.; supervision, F.D., E.R.L., P.-J.A. and D.T. All authors have read and agreed to the published version of the manuscript.

Funding: This research received no external funding.

Institutional Review Board Statement: Not applicable.

Informed Consent Statement: Not applicable.

Data Availability Statement: Not applicable.

Conflicts of Interest: The authors declare no conflict of interest.

Abbreviations and Symbols

BO	Bayesian Optimization
EGO	Efficient Global Optimization
FE	Finite Element
JC	Johnson–Cook
RMS	Root Mean Square
$\mathcal{D}$	Set of samples
$\mathcal{M}$	Gaussian regression surrogate model
$\mathbb{R}$	Set of real numbers
A	Yield stress of the material
B	Modulus of strain hardening
C	Strain rate sensitivity
E (GPa)	Young's modulus of the material
h	Uncut chip thickness
m	Thermal softening exponent
n	Strain-hardening exponent
T	Current temperature
B_1	First set of bounds
B_2	Second set of bounds
F_c	Cutting force
F_f	Feed force
h'	Chip thickness
T_{melt}	Melting temperature of the material
T_{room}	Room temperatures of the material
V_c	Cutting speed
$(\alpha(\boldsymbol{x}))$	Acquisition function
$\boldsymbol{e}$	Error term or noise prediction
$F(\boldsymbol{x})$	Objective function
μ	Coulomb's friction coefficient
Δ_x	Difference with the experimental reference
ρ (kg/m3)	Density of the material
ν	Poisson's ratio
σ	Flow stress
ε	Strain
$\dot{\varepsilon}$	Strain rate
$\dot{\varepsilon_0}$	Reference strain rate
$\in$	Element of
$EI(\boldsymbol{x})$	Expected Improvement
$\boldsymbol{\omega}$	Weights Gaussian distribution term
y^*	Best current objective value
$y_{pred}(x)$	Prediction of $\boldsymbol{x}$ from the surrogate model
$\sigma(x)$	Standard deviation

Φ	Cumulative density function of $\mathcal{N}(0,1)$
ϕ	Probability density function
$K = \mathbf{\Phi}^T \Sigma \mathbf{\Phi}$	Covariance matrix

References

1. Arrazola, P.; Özel, T.; Umbrello, D.; Davies, M.; Jawahir, I. Recent advances in modelling of metal machining processes. *CIRP Ann.—Manuf. Technol.* **2013**, *62*, 695–718. [CrossRef]
2. Furrer, D.; Semiatin, S. *Metals Process Simulation*; ASM International: Materials Park, OH, USA, 2010. [CrossRef]
3. Pimenov, D.; Guzeev, V. Mathematical model of plowing forces to account for flank wear using FME modeling for orthogonal cutting scheme. *Int. J. Adv. Manuf. Technol.* **2017**, *89*, 3149–3159. [CrossRef]
4. Yi, J.; Zhou, W.; Deng, Z. Experimental Study and Numerical Simulation of the Intermittent Feed High-Speed Grinding of TC4 Titanium Alloy. *Metals* **2019**, *9*, 802. [CrossRef]
5. Markopoulos, A. *Finite Element Method in Machining Processes*; ASM International: Materials Park, OH, USA, 2012. [CrossRef]
6. Ducobu, F.; Rivière-Lorphèvre, E.; Filippi, E. Application of the Coupled Eulerian-Lagrangian (CEL) method to the modeling of orthogonal cutting. *Eur. J. Mech. A/Solids* **2016**, *59*, 58–66. [CrossRef]
7. Kugalur-Palanisamy, N.; Riviere-Lorphèvre, E.; Arrazola, P.J.; Ducobu, F. Comparison of Johnson-Cook and modified Johnson-Cook material constitutive models and their influence on finite element modelling of Ti6Al4V orthogonal cutting process. *AIP Conf. Proc.* **2019**, *2113*, 80009. [CrossRef]
8. Melkote, S.; Grzesik, W.; Outeiro, J.; Rech, J.; Schulze, V.; Attia, H.; Arrazola, P.; M'Saoubi, R.; Saldana, C. Advances in material and friction data for modelling of metal machining. *Cirp Ann.—Manuf. Technol.* **2017**, *66*, 731–754. [CrossRef]
9. Kugalur-Palanisamy, N.; Rivière-Lorphèvre, E.; Arrazola, P.J.; Ducobu, F. Influence of Coulomb's Friction Coefficient in Finite Element Modeling of Orthogonal Cutting of Ti6Al4V. In Proceedings of the 25th International Conference on Material Forming, Braga, Portugal, 27–29 April 2022.
10. Childs, T. Friction modelling in metal cutting. *Wear* **2006**, *260*, 310–318. [CrossRef]
11. Qian, X.; Duan, X. Constitutive Model and Cutting Simulation of Titanium Alloy Ti6Al4V after Heat Treatment. *Materials* **2019**, *12*, 4145. [CrossRef]
12. Chandrasekaran, H.; M'Saoubi, R.; Chazal, H. Modelling of material flow stress in chip formation process from orthogonal milling and split hopkinson bar tests. *Mach. Sci. Technol.* **2005**, *9*, 131–145. [CrossRef]
13. Sterle, L.; Pušavec, F.; Kalin, M. Determination of friction coefficient in cutting processes: comparison between open and closed tribometers. *Procedia CIRP* **2019**, *82*, 101–106. [CrossRef]
14. Malakizadi, A.; Hosseinkhani, K.; Mariano, E.; Ng, E.; del prete, A.; Nyborg, L. Influence of friction models on FE simulation results of orthogonal cutting process. *Int. J. Adv. Manuf. Technol.* **2017**, *88*, 3217–3232. [CrossRef]
15. Sahoo, P.; Patra, K.; Singh, V.K.; Gupta, M.K.; Song, Q.; Mia, M.; Pimenov, D.Y. Influences of TiAlN coating and limiting angles of flutes on prediction of cutting forces and dynamic stability in micro milling of die steel (P-20). *J. Mater. Process. Technol.* **2020**, *278*, 116500. [CrossRef]
16. Özel, T.; Altan, T. Determination of workpiece flow stress and friction at the chip–tool contact for high-speed cutting. *Int. J. Mach. Tools Manuf.* **2000**, *40*, 133–152. [CrossRef]
17. Shrot, A.; Bäker, M. Determination of Johnson–Cook parameters from machining simulations. *Comput. Mater. Sci.* **2012**, *52*, 298–304. [CrossRef]
18. Klocke, F.; Lung, D.; Buchkremer, S.; Jawahir, I.S. From Orthogonal Cutting Experiments towards Easy-to-Implement and Accurate Flow Stress Data. *Mater. Manuf. Process.* **2013**, *28*, 1222–1227. [CrossRef]
19. Bosetti, P.; Bort, C.M.G.; Bruschi, S. Identification of Johnson–Cook and Tresca's Parameters for Numerical Modeling of AISI-304 Machining Processes. *J. Manuf. Sci. Eng.* **2013**, *135*, 51021. [CrossRef]
20. Denkena, B.; Grove, T.; Dittrich, M.; Niederwestberg, D.; Lahres, M. Inverse Determination of Constitutive Equations and Cutting Force Modelling for Complex Tools Using Oxley's Predictive Machining Theory. *Procedia CIRP* **2015**, *31*, 405–410. [CrossRef]
21. Bergs, T.; Hardt, M.; Schraknepper, D. Inverse material model parameter identification for metal cutting simulations by optimization strategies. *MM Sci. J.* **2019**, *2019*, 3172–3178. [CrossRef]
22. Bergs, T.; Hardt, M.; Schraknepper, D. Determination of Johnson-Cook material model parameters for AISI 1045 from orthogonal cutting tests using the Downhill-Simplex algorithm. *Procedia Manuf.* **2020**, *48*, 541–552. [CrossRef]
23. Hardt, M.; Schraknepper, D.; Bergs, T. Investigations on the Application of the Downhill-Simplex-Algorithm to the Inverse Determination of Material Model Parameters for FE-Machining Simulations. *Simul. Model. Pract. Theory* **2021**, *107*, 102214. [CrossRef]
24. Hardt, M.; Jayaramaiah, D.; Bergs, T. On the Application of the Particle Swarm Optimization to the Inverse Determination of Material Model Parameters for Cutting Simulations. *Modelling* **2021**, *2*, 129–148. [CrossRef]
25. Hardt, M.; Bergs, T. Considering multiple process observables to determine material model parameters for FE-cutting simulations. *Int. J. Adv. Manuf. Technol.* **2021**, *113*, 3419–3431. [CrossRef]
26. Jones, D.R.; Schonlau, M.; Welch, W.J. Efficient Global Optimization of Expensive Black-Box Functions. *J. Glob. Optim.* **1998**, *13*, 455–492. [CrossRef]

27. Briffoteaux, G.; Gobert, M.; Ragonnet, R.; Gmys, J.; Mezmaz, M.; Melab, N.; Tuyttens, D. Parallel surrogate-assisted optimization: Batched Bayesian Neural Network-assisted GA versus q-EGO. *Swarm Evol. Comput.* **2020**, *57*, 100717. [CrossRef]
28. Ducobu, F.; Rivière-Lorphèvre, E.; Filippi, E. On the introduction of adaptive mass scaling in a finite element model of Ti6Al4V orthogonal cutting. *Simul. Model. Pract. Theory* **2015**, *53*, 1–14. [CrossRef]
29. Arrazola, P.J.; Özel, T. Investigations on the effects of friction modeling in finite element simulation of machining. *Int. J. Mech. Sci.* **2010**, *52*, 31–42. [CrossRef]
30. Johnson, G.R.; Cook, W.H. A constitutive model and data for metals subjected to large strains, high strain rates and high temperatures. *Eng. Fract. Mech.* **1983**, *21*, 31–48. [CrossRef]
31. Childs, T.H.C. Material property needs in modeling metal machining. *Mach. Sci. Technol.* **1998**, *2*, 303–316. [CrossRef]
32. Ducobu, F.; Arrazola, P.J.; Rivière-Lorphèvre, E.; de Zarate, G.O.; Madariaga, A.; Filippi, E. The CEL Method as an Alternative to the Current Modelling Approaches for Ti6Al4V Orthogonal Cutting Simulation. *Procedia Cirp* **2017**, *58*, 245–250. [CrossRef]
33. Kugalur Palanisamy, N.; Rivière Lorphèvre, E.; Arrazola, P.J.; Ducobu, F. Influence of Constitutive Models and the Choice of the Parameters on FE Simulation of Ti6Al4V Orthogonal Cutting Process for Different Uncut Chip Thicknesses. *J. Manuf. Mater. Process.* **2021**, *5*, 56. [CrossRef]
34. Calamaz, M.; Coupard, D.; Girot, F. A new material model for 2D numerical simulation of serrated chip formation when machining titanium alloy Ti–6Al–4V. *Int. J. Mach. Tools Manuf.* **2008**, *48*, 275–288. [CrossRef]
35. Sima, M.; Ozel, T. Modified material constitutive models for serrated chip formation simulations and experimental validation in machining of titanium alloy Ti–6Al–4V. *Int. J. Mach. Tools Manuf.* **2010**, *50*, 943–960. [CrossRef]
36. Markopoulos, A.; Vaxevanidis, N.; Manolakos, D. Friction and Material Modelling in Finite Element Simulation of Orthogonal Cutting. *Tribol. Ind.* **2015**, *37*, 440–448.
37. Shahriari, B.; Swersky, K.; Wang, Z.; Adams, R.P.; de Freitas, N. Taking the Human Out of the Loop: A Review of Bayesian Optimization. *Proc. IEEE* **2016**, *104*, 148–175. [CrossRef]
38. Rasmussen, C.E.; Williams, C.K.I. *Gaussian Processes for Machine Learning (Adaptive Computation and Machine Learning)*; MIT Press: Cambridge, MA, USA, 2005.
39. Ducobu, F.; Riviere, E.; Filippi, E. Experimental contribution to the study of the Ti6Al4V chip formation in orthogonal cutting on a milling machine. *Int. J. Mater. Form.* **2014**, *8*, 455–468. [CrossRef]
40. Movahhedy, M.R.; Gadala, M.S.; Altintas, Y. Simulation of chip formation in orthogonal metal cutting process: An ale finite element approach. *Mach. Sci. Technol.* **2000**, *4*, 15–42. [CrossRef]
41. Agode, K.; Wolff, C.; Nouari, M.; Moufki, A. Microstructure scale modelling of the WC and Co phases plastic behaviour in the WC-Co composite with different cobalt contents and for different temperatures. Comparison of the Drucker-Prager and Mises models. *Int. J. Refract. Met. Hard Mater.* **2021**, *99*, 105588. [CrossRef]
42. Gerd Lütjering, J.C.W. *Titanium*; Springer: Berlin/Heidelberg, Germany, 2007.
43. Leseur, D. *Experimental Investigations of Material Models for Ti-6A1-4V and 2024-T3*; Lawrence Livermore National Lab.: Livermore, CA, USA, 1999. [CrossRef]
44. Boivineau, M.; Cagran, C.; Doytier, D.; Eyraud, V.; Nadal, M.H.; Wilthan, B.; Pottlacher, G. Thermophysical Properties of Solid and Liquid Ti–6Al–4V (TA6V) Alloy. *Int. J. Thermophys.* **2006**, *27*, 507–529. [CrossRef]
45. Callister, W.D. *Materials Science and Engineering: An Introduction*; Wiley: Hoboken, NJ, USA, 1996.
46. Seo, S.; Min, O.; Yang, H. Constitutive equation for Ti–6Al–4V at high temperatures measured using the SHPB technique. *Int. J. Impact Eng.* **2005**, *31*, 735–754. [CrossRef]
47. Iman, R.L. Latin Hypercube Sampling. In *Encyclopedia of Quantitative Risk Analysis and Assessment*; John Wiley & Sons, Ltd.: Hoboken, NJ, USA, 2008. [CrossRef]
48. Sammut, C.; Webb, G.I. (Eds.) Leave-One-Out Cross-Validation. In *Encyclopedia of Machine Learning*; Springer: Boston, MA, USA, 2010; pp. 600–601. [CrossRef]
49. Gardner, J.R.; Pleiss, G.; Bindel, D.; Weinberger, K.Q.; Wilson, A.G. GPyTorch: Blackbox Matrix-Matrix Gaussian Process Inference with GPU Acceleration. In Proceedings of the Advances in Neural Information Processing Systems, Montreal, QC, Canada, 2–8 December 2018.
50. Gobert, M.; Gmys, J.; Toubeau, J.F.; Vallée, F.; Melab, N.; Tuyttens, D. Surrogate-Assisted Optimization for Multi-stage Optimal Scheduling of Virtual Power Plants. In Proceedings of the 2019 International Conference on High Performance Computing Simulation (HPCS), Dublin, Ireland, 15–19 July 2019; pp. 113–120. [CrossRef]